Plasticity Variable Collagen-PEG Interpenetrating Networks Modulate Cell Spreading

Iris G. Mercer¹, Karen Yu¹, Alexander J. Devanny¹, Melissa B. Gordon², Laura J. Kaufman^{1,*}

ABSTRACT

The extracellular matrix protein collagen I has been used extensively in the field of biomaterials due to its inherent biocompatibility and unique viscoelastic and mechanical properties. Collagen I self-assembly into fibers and networks is environmentally sensitive to gelation conditions such as temperature, resulting in gels with distinct network architectures and mechanical properties. Despite this, collagen gels are not suitable for many applications given their relatively low storage modulus. We have prepared collagen-poly(ethylene glycol) [PEG] interpenetrating network (IPN) hydrogels to reinforce the collagen network, which also induces changes to network plasticity, a recent focus of study in cell-matrix interactions. Here, we prepare collagen/PEG IPNs varying collagen concentration and collagen gelation temperature to assess changes in microarchitecture and mechanical properties of these networks. By tuning these parameters, IPNs with a range of stiffness, plasticity and pore size are obtained. Cell studies suggest that matrix plasticity is a key determinant of cell behavior, including cell elongation, on these gels. This work presents a natural/synthetic biocompatible matrix that retains the unique structural properties of collagen networks with increased storage modulus and tunable plasticity. The described IPN materials will be of use for applications in which control of cell spreading is desirable, as only minimal changes in sample preparation lead to changes in cell spreading and circularity. Additionally, this study contributes to our understanding of the connection between collagen self-assembly conditions and matrix structural and mechanical properties and presents them as useful tools for the design of other collagen based biomaterials.

¹ Department of Chemistry, Columbia University, New York, NY 10025

² Department of Chemical and Biomolecular Engineering, Lafayette College, Easton, PA 18042

^{*}corresponding author

1. INTRODUCTION

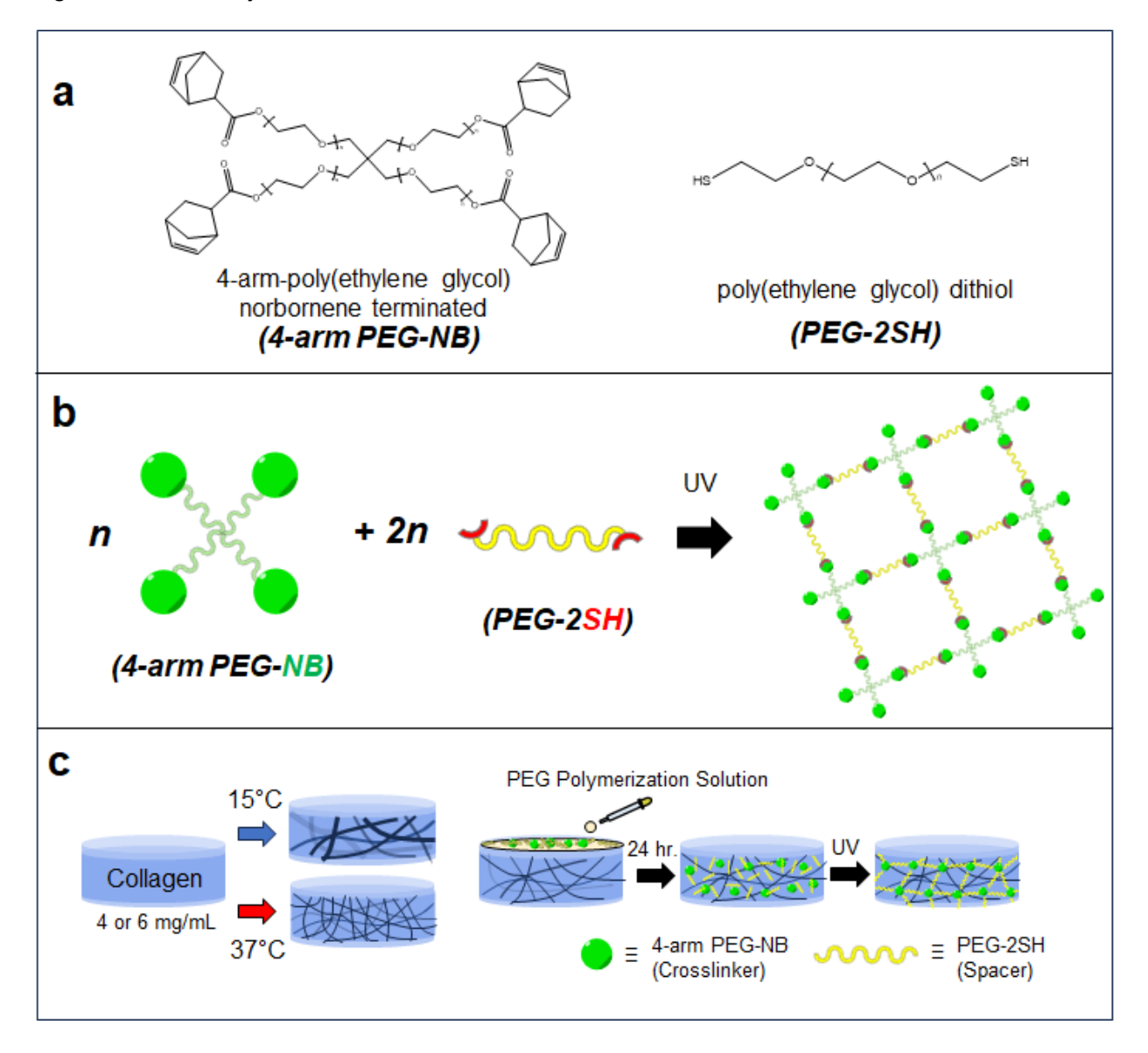
Biomaterials are a diverse class of materials composed of and/or designed to interact with biological systems. Biomaterials can be designed not only for biocompatibility but also for other properties including bioactivity, biodegradability, and specific mechanical or structural properties, lending them great versatility of end uses. One strategy that has been utilized in biomaterial design is mimicking components of the native cellular environment. Such biomimetic materials often replicate properties of the extracellular matrix (ECM), maintaining its biocompatibility and important functions in cell regulation while adding desired properties or functionality.

Interpenetrating polymer networks (IPN) have grown in popularity as biomaterials, as they can recapitulate key aspects of the complex environment of the ECM. IPNs are complexes of two or more independent networks that are interlaced or physically entangled but lack covalent interactions[1,2]. IPNs that include a biological network component typically provide mechanical reinforcement while preserving native architecture of the network[3,4]. Being the predominant structural and functional component of mammalian ECM, collagen I has long been used in biomaterials for bioengineering applications and biophysical studies[5] and has recently found use as a component in IPNs[6–9]. Among collagen-based IPN biomaterials, some have utilized a reactive poly(ethylene glycol) (PEG) to form the secondary network, resulting in hydrogels useful for both cellular studies and tissue engineering scaffolds [8–10]. These studies have shown collagen-PEG IPNs support cell viability and that modifications to the PEG network can modulate cell response, including proliferation, extent of cell spreading, and migration. Most of the exploration of collagen-PEG IPNs to date has been through alterations to the PEG network, whereas little attention has been given to modification of the primary collagen network, despite its importance in cell adhesion and signaling and its high sensitivity to gelation conditions[11,12].

Collagen I in its monomeric form is a left handed helix composed of three polypeptide chains, two of which are distinct[13]. Both in vivo and in vitro it can self-assemble in an entropically driven process into fibrils that may further bundle into fibers that can associate to produce a hydrogel[14,15]. Collagen I self-assembly kinetics and hydrogel equilibrium properties are sensitive to gelation conditions including concentration, pH, temperature, and type of collagen. These properties can each affect fibril number and morphology and ultimately network properties, including pore size and stiffness[16–19]. It has been shown that changes in collagen network structure correspond to distinct cellular behaviors - for example, for collagen I gels of moderate to high concentration, self-assembly at lower temperatures supports enhanced cell invasion due to increased pore size relative to that present in gels that self-assemble at physiological temperature[20]. As such, gelation conditions can be tuned to lend collagen hydrogels targeted network properties and biological function. Here, we show that the environmental sensitivity of the collagen primary network is retained in a collagen/PEG IPN, allowing enhanced variation of network structure and mechanical properties of such networks and further study of cell response to a variety of mechano-structural properties.

In the study of cell-matrix interactions, recent attention has been placed on the importance of mechanical properties, in particular matrix plasticity[21–24], as determinants of cell behavior not only in vitro but also in vivo. We prepared collagen-PEG IPN hydrogels (**Scheme 1**) to explore the extent to which collagen gelation parameters affect the material's bulk properties including plasticity and cell spreading behavior. The temperature of collagen gelation and the concentration of collagen was varied to create IPNs with a wide range of storage modulus, plasticity, and pore size. While it has been shown that collagen/PEG IPNs can support cell survival, proliferation, and differentiation within the 3D gel [8–10], here we interrogate cell behavior atop the 2D substrates. Such measurements, while lacking some complexity of the 3D environment cells experience in

vivo, are commonly used in fundamental studies of mechanobiology[25] and allow interrogation of cell response to materials with distinct mechanical properties without significant influence of pore size, a key determinant of cell behavior within 3D networks[20,26–29]. Experiments with both dispersed cells and cells cultured as spheroids atop the IPNs explored here show that within collagen/PEG IPNs, collagen concentration and gelation temperature can limit or enhance cellular spreading and elongation, apparently through differences in IPN plasticity. This study demonstrates that the collagen-PEG hydrogel system can be tuned towards specific desired structural and mechanical properties as well as cellular responses by modifying the primary collagen network. This demonstration and exploration of tunable collagen IPNs elucidates the role of plasticity in cell behavior and will be of value for the design of collagen-based biomaterials with targeted functionality.



Scheme 1. Graphical depiction of collagen-PEG IPNs. a) Chemical structures of PEG-NB and PEG-2SH. **b)** Reaction scheme for the secondary network of the collagen-PEG IPN and PEG hydrogels. Thiolene click chemistry is used to polymerize norbornene functional groups on the four-armed crosslinker with dithiol groups on the PEG spacer (highlighted in green and red, respectively). The two reactants are utilized in a 1:2 stoichiometric ratio of crosslinker to spacer. An idealized diagram of the resulting network is

presented. **c)** For the primary network, collagen hydrogels are formed at different concentrations and gelation temperatures leading to hydrogels of varied stiffness and pore size. The PEG solution is placed on top of the collagen gel and allowed to diffuse for 24 hours, after which polymerization is initiated with lrgacure 2959 and fifteen minutes of UV exposure.

2. MATERIALS AND METHODS

2.1 PEG-norbornene solution

4-arm poly(ethylene glycol) norbornene terminated ($\overline{M_n}$ = 10,000 g/mol) and poly(ethylene glycol) dithiol ($\overline{M_n}$ = 3,400 g/mol) were purchased from ThermoFisher and prepared in a 2.5:5 mM ratio, respectively, along with 1% w/w of initiator 2-hydroxy-4'-(2-hydroxyethoxy)-2-methylpropiophenone (Irgacure 2959, ThermoFisher). Reagents and solutions were stored under nitrogen when not in use.

2.2 Hydrogel preparation

Hydrogels were prepared in circular plastic 25 mm diameter molds in order to match the size of the parallel plate geometry used for rheological tests.

For PEG-only gels, 600µL of the PEG-norbornene (PEG-NB) solution was dispensed into the mold and immediately UV cured for 15 minutes, after which it was washed two times with 1X PBS.

For collagen-only gels, 10 mg/mL acid-solublized rat tail collagen (Ratcol, Advanced BioMatrix) was diluted with 20mM acetic acid to a final concentration of 6 mg/mL or 4 mg/mL Ratcol (Advanced BioMatrix) to create high concentration and low concentration collagen gels, respectively. The concentration of collagen in the final preparation for the high and low concentration gels was 5.4 mg/mL and 3.6 mg/mL, respectively, although concentrations throughout the paper will refer to the concentration of stock solution employed. 540 μ L of collagen solution was neutralized in a 1.5-mL microcentrifuge tube with a neutralization solution of 10X PBS and sodium hydroxide to a final pH of 7.2-7.4 and volume of 600 μ L, and kept on ice for approximately five minutes before the solution was deposited into the mold. The mold was then placed in a 60mm plastic dish with a drop of water and covered with Parafilm to prevent drying before being placed in an incubator either at 37°C for 2 hours or 15°C overnight.

For IPN gels (**Scheme 1**), collagen was first prepared as described in the previous paragraph. After the gelation period, 400µL of the PEG-norbornene solution was dispensed onto the gel such that it evenly spread over the surface. After wrapping the outer dish in foil to prevent polymerization initiation from ambient light, the gel sat overnight at room temperature to allow the PEG-NB solution to diffuse through the collagen gel. After this period, excess solution was gently wicked off and the gel was washed with 1X PBS two times before placing it under UV light for 15 minutes, followed by two more washes with 1X PBS after curing.

After preparing either single component gels or IPNs as described above, the gels were removed from their molds with a stainless steel spatula. They were flipped such that the inner-mold side of the gel faced up towards the measuring plate of the rheometer. Any remaining liquid was wicked away prior to testing.

To prepare fluorescently labeled collagen for imaging collagen and IPN gels, a stock of AlexaFluor 555 (Thermo Fisher) labeled rat tail collagen was prepared as previously described[30,31] and mixed with unlabeled collagen to obtain 6 mg/mL and 4 mg/mL stock solutions. A custom mold

was fabricated to allow for imaging the gels without removing them from the mold and potentially perturbing the network structure. This entailed attaching a 25mm rubber gasket to a glass coverslip with UV glue. Otherwise, the gels were prepared as described above.

For IPNs used for spheroid deformation and relaxation measurements, Nile Red labeled 1 μ m diameter FluoSphere bead suspension (Invitrogen) was diluted in 60 μ L of neutralization solution to a final concentration of 6 \times 10¹⁰ beads/mL and then added to 540 μ L of collagen solution. The collagen network and subsequent IPN gels were then prepared as previously described.

2.3 Rheology

All rheological tests were performed on an Anton-Paar MCR302 rheometer with a 25-mm stainless steel parallel plate geometry with sandpaper affixed as the top plate and a glass bottom plate. Rather than gap size control, the measurement gap was set and maintained using normal force control to a constant normal force of 0.05N both to prevent sample slip and to account for potential deviations in sample height that would otherwise change the gap size. Storage modulus and loss modulus were measured in strain controlled mode by oscillatory shear with 0.1% strain and 1 Hz oscillations. Creep and recovery tests were performed in stress-controlled mode by applying a constant stress for 30 minutes followed by a recovery period (stress = 0 Pa) of up to an hour or until strain reached a plateau value and appeared to no longer be evolving. The plasticity of the hydrogels was determined from creep tests as $\varepsilon_{irr}/\varepsilon_{max}$ where ε_{max} is the maximum strain after creep and ε_{irr} is the irreversible strain after recovery, as defined by Nam et. al[21].

2.4 Cell Culture and Spheroid Preparation

MDA-MB-231 breast cancer cells were obtained from the American Type Culture Collection. DMEM high glucose liquid media and phosphate buffered saline (PBS) were obtained from GE Healthcare HyClone. Fetal bovine serum (FBS) was obtained from Gibco. Accutase and 100x penicillin-streptomycin-amphotericin B were obtained from MP Biomedicals. 100x MEM nonessential amino acid solution was obtained from Corning (Corning, NY). Matrigel growth factor reduced basement membrane extract (BME) and Cell Recovery Solution were obtained from Corning. ATTO-488 phalloidin and DAPI were obtained from Sigma Aldrich. LIVE/DEAD Cell Imaging Kit (488/570) was obtained from Molecular Probes by Thermo Fisher Scientific. CellTracker Green CMFDA was obtained from Invitrogen Life Technologies.

Cells were cultured on tissue culture plastic in 1× high glucose DMEM containing 10% (v/v) fetal bovine serum, 1% (v/v) 100× antibiotics solution, and 1% (v/v) 100× MEM non-essential amino acids solution. Cells were maintained at 37 $^{\circ}$ C under 5% carbon dioxide. Cells were sub-cultured when 80–90% confluency was reached and were used from passages 3–20.

Cells originally plated on tissue culture plastic were detached using Accutase. Cells were then counted and diluted in DMEM growth culture medium to 100,000 cells/mL. For studies of dispersed cells on gels, 1.5mL of the cell solution was placed atop the gels. These were then placed into the incubator at 37 °C under 5% carbon dioxide.

For spheroid formation, 2000 cells were placed in wells of an ultra-low adhesion 96-well plate in media supplemented with 0.2575 mg/mL BME. Plates were centrifuged for 10 minutes at 1000 x g. The cells were allowed to compact for 24-48 hours to form spheroids. Before imaging, spheroids were placed in Cell Recovery Solution on ice for 45-60 minutes to remove the BME.

2.5 Cell Attachment, Viability, and Shape Analysis

For dispersed cells atop gels, cell attachment was assessed by incubating cells with CellTracker Green for 45 minutes at a concentration of 2μ M. 150,000 cells were then plated on the gels and allowed to attach. After 24 hours, the gels were rinsed with PBS and fixed with 10% formalin (Thermo Fisher Scientific). Samples were then imaged with a 10X (NA = 0.4) objective on a Zeiss LSM800 microscope and manually counted.

Cell viability was separately assessed via live/dead imaging after 24 hours. Live Green and Dead Red stain vials were mixed and the solution was placed atop the cells and incubated at room temperature for 15 minutes. Samples were then imaged with a 10X (NA = 0.4) objective on a Zeiss LSM800 microscope. Live and dead cells were manually counted.

For cell shape analysis, at 24 hours after plating, cells were fixed with warmed 10% formalin for 10 minutes and then permeabilized with 0.2% Triton X-100 (EMD Millipore Chemicals) for 10 minutes. Cells were stained using ATTO 488 phalloidin (1:400) and DAPI (1:1000) in PBS overnight at 4°C. Images were taken on the 10X air (NA 0.4) and 20X air (NA 0.75) objectives of the Zeiss LSM800 inverted confocal microscope with 405 nm and 488 nm excitation lasers. When collagen was simultaneously imaged in such gels, a 555 nm excitation laser was additionally used. Cells were manually segmented and cell shape was quantified via circularity using ImageJ.

2.6 Spheroid Deformation and Relaxation Analysis

Spheroids were placed atop low and high collagen concentration IPN gels and imaged every two hours for 20 hours. After 20 hours, media was removed and replaced with a solution of 5μ M cytochalasin-D (Sigma Aldrich) and 1% Triton X-100 in culture media. Images were then taken every hour for up to six hours, though all relaxation was found to occur in the first hour after application of the relaxation solution. Throughout the experiments samples were held in an incubator at 37° C with 5% CO₂. Imaging was performed on a Zeiss Elyra 7 microscope with a 10x air (NA 0.3) objective. Z-stacks were taken at 10μ m intervals to 200μ m below the top of the gel.

Composite superimposed images of the bead-embedded gels were created using images taken directly after the addition of a spheroid and 20 hours after spheroid placement to quantify gel deformation. Composite images of the same type were created using images taken 20 hours after spheroid placement and two hours after application of cytochalasin-D to quantify relaxation. The images were drift-corrected with ImageJ using positions of beads in the lowest collected z-slice (approximately 200 µm below the top of the gel) to account for potential sample drift due to perturbation upon addition of the relaxation solution. Motion of at least 150 beads per sample visible in the top slice of the gels was quantified. Vectors were drawn in ImageJ between beads at the earlier and later time points for both pulling and relaxation ensuring that only readily identifiable and distinguishable beads were chosen. Bead displacement was then measured using ImageJ.

2.7 Pore Size Determination

For pore size determination, collagen imaging was performed on a Zeiss LSM800 inverted confocal laser scanning microscope with a 555 nm excitation laser using a 63X oil (NA 1.4) objective in Airyscan mode. Pore size was determined as previously described[32]. Single confocal slices of collagen gels and IPNs were pre-processed in ImageJ to yield a segmented image that was then used for pore size determination. Raw images were subjected to a bandpass filter and rolling ball background subtraction to remove features below a certain size threshold and reduce out of plane background signal, respectively. A local auto threshold was then used to obtain a binarized image of the network. Distances between "on" pixels were counted row by row and column by column in the segmented image. The distribution of gaps between fibers was fit to an exponential probability density function $f(x) = \lambda \times e^{-\lambda x}$. The characteristic pore size for the

network is $1/\lambda$. Results from multiple images taken at different locations in a sample were averaged together to determine a mean pore size for the sample, and this was repeated on n > 3 samples.

2.8 Statistical Analysis

Creep and recovery tests and cell attachment, viability, and shape tests were repeated at least three times each on independent samples, with the latter three additionally being conducted on different batches of cells on different days. Oscillatory shear experiments for viscoelastic moduli of PEG, collagen and IPN gels were performed at least ten times for each sample type. Sample sizes per replicate of cell experiments included over 160 cells each for cell viability assay, over thirty cells each for cell shape analysis, and five tiles of $\sim 0.4 \text{ mm}^2$ each for cell attachment assays. Spheroid experiments were repeated three times each on low and high concentration IPN gels formed at 37°C. Welch's t-tests were performed for comparisons of storage moduli between collagen and IPN gels of identical temperature and collagen concentration, and ANOVA was used to compare storage moduli, pore sizes, cell viabilities and cell attachment counts amongst all sample types followed by post-hoc Tukey tests. Kolmogorov-Smirnov tests were performed to compare cell shape distributions. Indicated significance levels are as follows for all described tests: * \equiv p < 0.05, ** \equiv p < 0.01, *** \equiv p < 0.001. Unless otherwise mentioned, individual data points represent means and error bars represent standard deviations. Circularity distributions are presented with kernel smoothing via Origin Pro (v. 2024, Origin Labs).

3. RESULTS

Mechanical Properties of Single Component Hydrogels

First, the properties of the collagen primary network and PEG secondary network were characterized individually, by preparing collagen and PEG hydrogels separately. Collagen gels were prepared from stock solutions of 4 and 6 mg/mL and at gelation temperatures of 15°C and 37°C. The PEG hydrogels were prepared at a ratio of 2.5 mM 4-arm poly(ethylene glycol) norbornene terminated to 5 mM poly(ethylene glycol) dithiol. The dynamic storage and loss moduli, *G*' and *G*" respectively, of the hydrogels were obtained from oscillatory shear tests, and creep tests were performed over a range of applied stresses to obtain gel plasticity.

Storage moduli (G') of collagen gels were found to increase with increasing collagen concentration and decreasing gelation temperature, consistent with previous results[19] (Fig. 1a). Indeed, in this study, the low concentration collagen gelled at 15°C showed a similar stiffness to the high concentration collagen gelled at 37°C, with no significant difference between the two sample populations. Creep and recovery tests were performed to measure gel plasticity, a measure of the permanent, irreversible strain experienced in a gel after stress is applied for some time before the sample is allowed to recover towards its original state. Here, a constant stress was applied to the sample for 30 minutes and then removed, with percent strain monitored during stress application and relaxation, as described in Methods. This measurement revealed that both types of collagen gels displayed stress-dependent plasticity and, at all stresses measured, low concentration collagen hydrogels displayed a higher plasticity compared to the high concentration collagen hydrogels (Fig. 1b). As expected, the PEG hydrogels were the least plastic (most elastic) and showed a stress-independent response, as the covalent crosslinks in these networks limit plastic deformation relative to the weaker intermolecular interactions and physical entanglements in collagen networks that allow for dynamic rearrangement. While the PEG hydrogels did show the lowest plasticity, they displayed a higher degree of irreversible (plastic) deformation after creep and recovery tests than some covalently crosslinked synthetic networks. Plastic

deformation is possible in such networks due to, for example, sliding of crosslinks[33]. The relatively long timescale of the stress application (30 minutes) in these experiments and the relatively long length of the PEG spacer are likely responsible for the plasticity observed in these gels[34,35]; indeed, when using a shorter spacer or shorter creep loading times, the observed plasticity of the PEG gels decreased (**Fig. S1a,b**). Additionally, creep and recovery tests were performed on a highly crosslinked 10% polyacrylamide to assure our protocol reported results consistent with previous findings for highly elastic samples. The polyacrylamide gel was dominated by elastic behavior and showed virtually no irreversible strain following recovery (**Fig. S1c**).

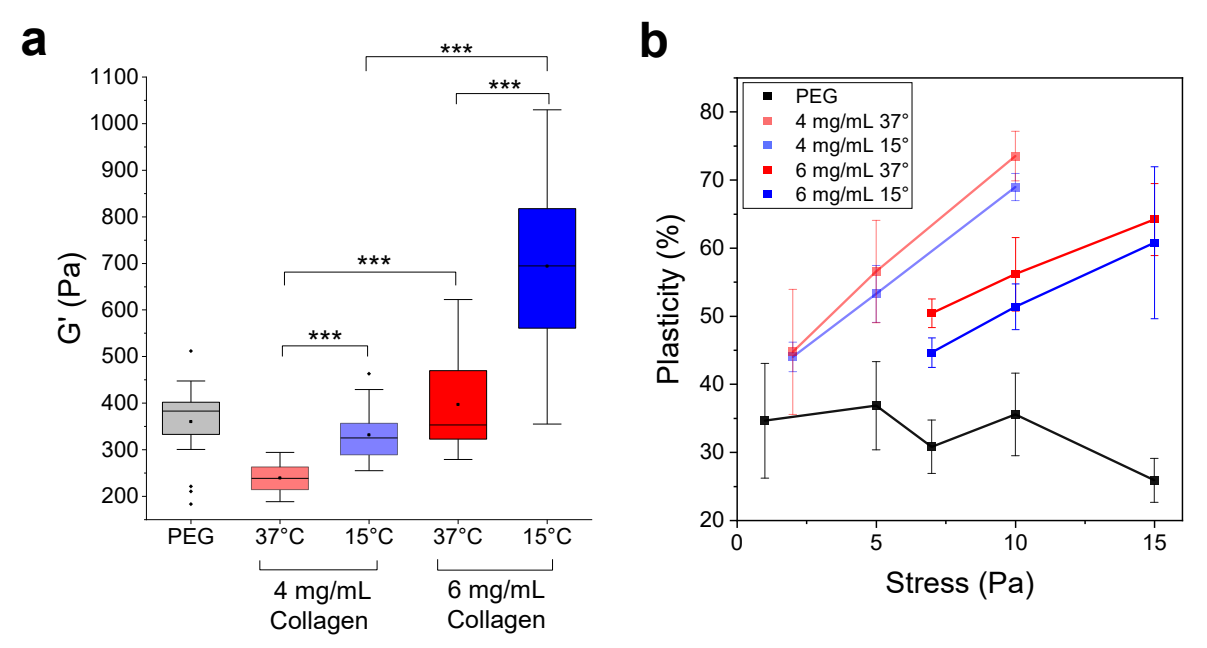


Figure 1. Rheology of collagen hydrogels as a function of gelation conditions. a) Storage moduli (G') of single-component hydrogels as determined by oscillatory rheology with $\gamma = 0.1\%$, f = 1 Hz. ($n \ge 19$, *** $\equiv p < 0.001$). b) Plasticity of independent hydrogels as determined by creep and recovery tests at different applied stresses (Pa) ($n \ge 3$).

Creep and recovery tests were performed over a range of stresses to assess how the magnitude of applied stress affects the plasticity of the networks, as stress-dependent plasticity is a feature of collagen networks but not of most synthetic networks and some other biopolymer networks[21]. The stress ranges interrogated were chosen based on the lowest stress producing reproducible results and the highest before sample breakage, also ensuring that all samples had portions of overlapping stresses probed for comparison. The collagen hydrogels displayed stress- dependent plasticity, while PEG hydrogels displayed constant plasticity over the range tested. The nonlinear viscoelasticity of collagen gels as evidenced by the stress dependent plasticity is consistent with previous work by Nam et al.[21]. Here, we also show that higher concentration collagen I gels display lower plasticity and a lower degree of stress dependence than the lower concentration counterparts. The former finding is inconsistent with an earlier observation and model of collagen plasticity, though those experiments were performed over a greater concentration range and plasticity was not compared at the same stress across samples[36]. For the networks investigated here, we find that the plastic deformation of collagen gels is primarily dependent on the collagen concentration and not on gelation temperature, indicating plasticity is not strongly linked to differences in network structure in collagen gels, as those prepared at 15°C have increased fiber bundling and pore size relative to those of the same concentration prepared at 37°C[19]. While

these differences in network structure do not set differences in stress-dependent plasticity, they do effect differences in storage moduli between such networks at a given concentration (Fig. 1a).

Mechanical Properties and Network Architecture of IPNs

IPN hydrogels of collagen and PEG were then prepared using 4 mg/mL and 6 mg/mL collagen stock solutions and at collagen gelation temperatures of 15°C and 37°C as shown in **Scheme 1** and described in Methods. Thiol-ene polymerization functionalized PEG was chosen for this purpose, as it reacts bio-orthogonally given that the number of free thiol groups in most proteins, including collagen, is very low [37]. This ensures that the networks will be physically entangled rather than covalently attached and suggests the collagen network will remain unperturbed by the addition of the PEG. Following reinforcement with the PEG secondary network, the IPNs at all conditions were stiffer than their collagen counterparts as reported by oscillatory rheology (**Fig. 2a**). As with the pure collagen hydrogels, increase in concentration and decrease in gelation temperature both increase the storage moduli of the IPNs, suggesting that the structural changes that occur in pure collagen networks as a function of gelation conditions are maintained in the IPNs.

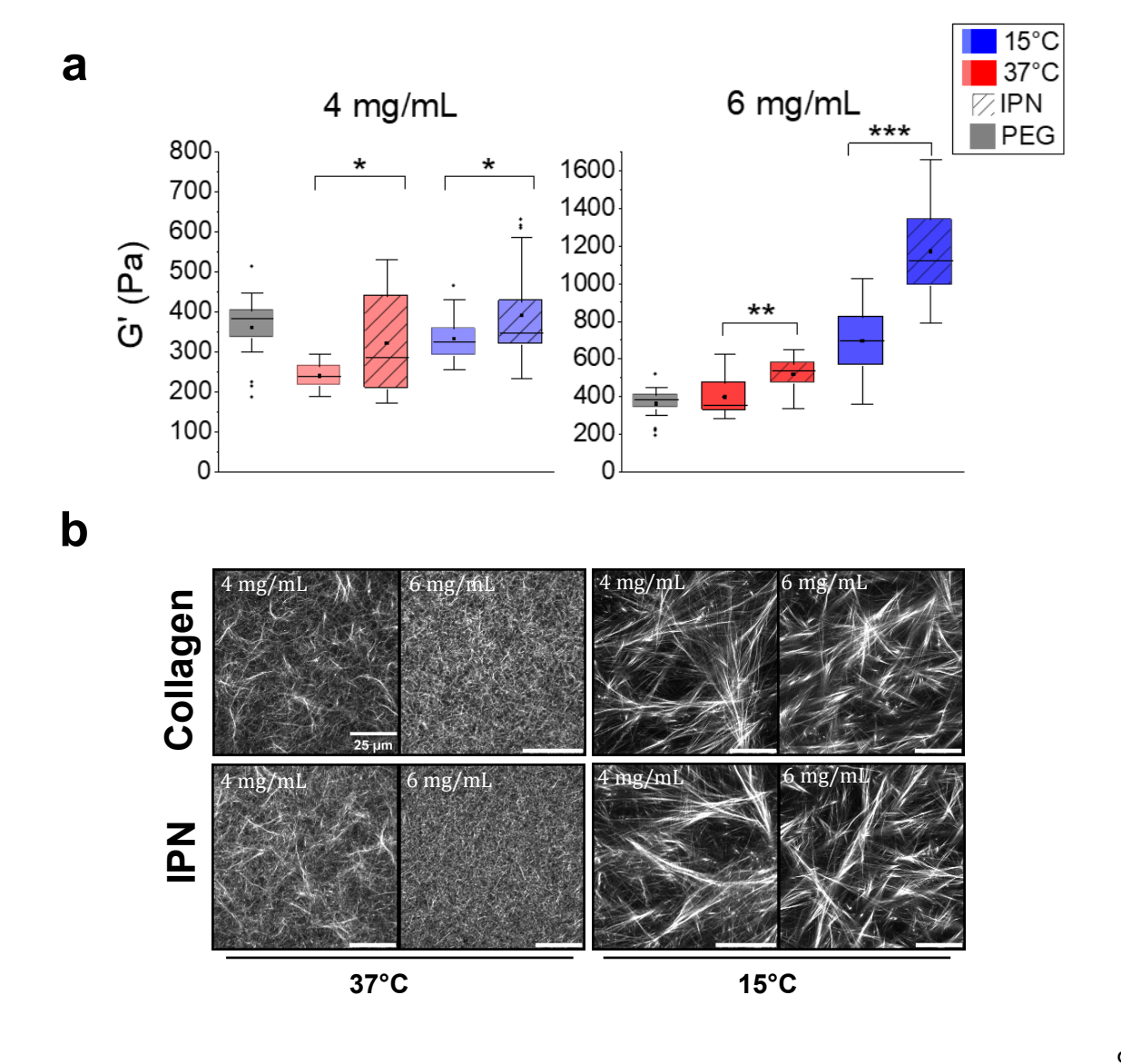


Figure 2. Storage moduli and network structure of IPNs. a) Storage moduli (G') of collagen-PEG IPN hydrogels (cross-hatched) compared to those of individual networks (solid fill) for the different collagen concentrations (left, 4 mg/ml, right, 6 mg/mL) and temperatures (blue, 15°C and red, 37°C). Pure PEG and collagen gel results are also shown in Fig. 1a. **b)** Airyscan images of (top row) collagen hydrogels and (bottom row) collagen-PEG IPN hydrogels at collagen concentrations of 4 and 6 mg/mL and gelation temperature of 15°C or 37°C. Scale bar = 25μm.

To confirm this hypothesis, Alexa Fluor 555 labeled collagen stock solutions were used to prepare both pure collagen hydrogels and collagen-PEG IPNs, and the samples' network architectures were visualized with Airyscan confocal fluorescence microscopy (CFM) (Fig. 2b). The images were analyzed for characteristic pore size across several positions per sample and across multiple (n > 3) samples. As expected based on previous results[19,20], pure collagen gels self-assembled at lower temperatures displayed collagen fiber bundling that results in a large increase in pore size relative to collagen gels of the same concentrations gelled at higher temperature. Collagen-PEG IPNs showed no significant structural differences from pure collagen gels formed at identical gelation conditions, both qualitatively via CFM images and quantitatively from pore size analysis (Fig. S2). We note that, with the exception of the 4 mg/mL and 6 mg/mL IPNs prepared at 15°C, there were no significant differences in pore size for gels formed at the same temperature despite differences in concentration, indicating temperature as a stronger determinant in network architecture than concentration in this narrow and relatively high concentration range. Critically, we have shown that creating the collagen-PEG IPN does not alter the network structure of the primary collagen network.

Given that the IPNs display similar changes in storage moduli and microstructure as a function of collagen concentration and gelation temperature as pure collagen gels, we explored whether the collagen network plasticity was retained in the IPNs. Creep and recovery tests performed on the IPNs showed a much broader range of plasticity amongst the IPNs compared to the pure collagen networks, with each IPN showing distinct response to deformation as seen via normalized strain curves (Fig. S3). These differences are further evident in creep tests across a range of applied stresses (Fig. 3), with each sample type displaying different degrees of stress- dependent plasticity, covering a broader range than seen in pure collagen gels (Fig. 1, Fig. S4).

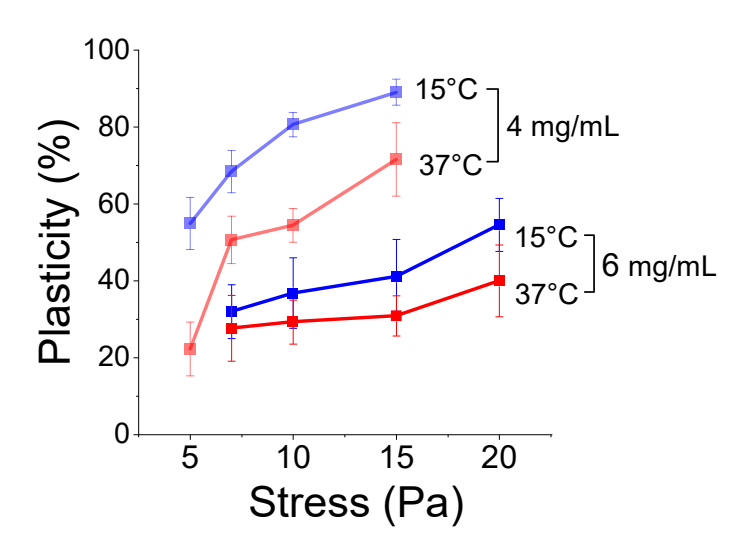


Figure 3. Stress-dependent plasticity of IPNs. Stress dependence of plasticity in collagen-PEG IPNs for each gelation condition. Stress indicates the magnitude of applied stress during the creep phase of creep-recovery experiments.

Cell Activity on IPNs

Next we explored how the material properties and architecture of the networks affect spreading behavior of MDA-MB-231 cells cultured atop the IPNs. Cell viability tests were first performed on pure collagen gels and the IPNs. In all cases, cell viability was nearly 100% and no significant difference in cell viability was seen with addition of the PEG secondary network (Fig. S5a). We then used Airyscan CFM to image cells atop the IPNs after they had been allowed to spread for 24 hours and analyzed cell shape. It was found that each collagen gelation condition led to diverse cell spreading behaviors on the IPNs (Fig. 4a). Cell shape distributions were found to be bimodal, with some cells spreading and displaying a spindle-like morphology and others remaining compact and nearly circular. To assess whether these differences could be due to differences in cell attachment propensity across the gels, a cell attachment assay was performed. No significant differences were found in cell attachment across the gels (Fig. S5b). The proportion of elongated cells correlated with the plasticity of the hydrogels; the hydrogel with the highest plasticity, the low concentration 15°C collagen IPN, had a large proportion of extended cells and a small proportion of circular cells, while the hydrogel least susceptible to plastic deformation, the high concentration 37°C collagen IPN, had a distribution skewed in the other direction, towards high circularity, round cells (Fig. 4b). This trend follows through the intermediate plasticity samples. In contrast, no clear relationship was found between IPN pore size and cell circularity, storage modulus and cell circularity, or loss modulus and cell circularity (Fig. S6).

Since it was observed that the IPNs were less plastic than the corresponding collagen gels, we also compared cell circularity distributions on the IPNs to those on collagen gels. In particular, we compared the high collagen concentration gels as those were clearly more plastic than their IPN counterparts (**Fig. S4**). Kernel density estimate plots of their distributions show that the collagen gels had similar distributions to the IPNs, but with greater proportion of elongated cells (**Fig. S7**). Together, these results support the assertion that plasticity is a key determinant of cell spreading and elongation in 2D in these IPNs.

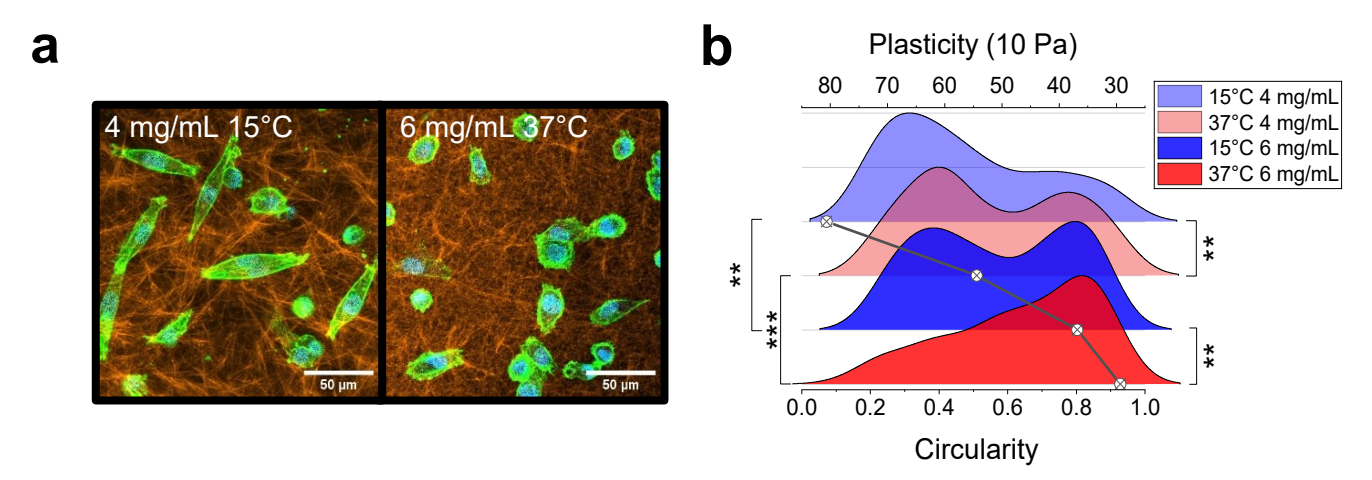


Figure 4. Collagen-PEG IPN plasticity modulates cell spreading. a) Representative images of MDA-MB-231 cells on (left) a highly plastic and (right) a highly elastic collagen-PEG IPN gel. **b)** Circularity distribution of cells incubated on collagen-PEG IPNs. Points represent mean plasticity of each gel from creep and recovery tests with an applied stress of 10 Pa ($n \ge 3$) (also shown in **Fig. 3**). Kolmogorov-Smirnov tests comparing the indicated distributions are shown (**p< 0.01 and ***p< 0.001).

To more directly tie the observed cell behavior to plasticity of the underlying gels and to confirm that cell activity provokes similar changes in gels as the macroscopic creep and recovery tests, we pursued additional cell experiments. Forces exerted by individual cells plated atop gels led to small gel deformations that were difficult to quantify. Instead, we quantified deformation induced by spheroids placed atop gels. Specifically, we placed spheroids atop fluorosphere-loaded IPNs of high and low collagen concentration formed at 37°C, since these gels had significant differences in plasticity as measured by creep and recovery tests (**Fig. 3**) and cell circularity (**Fig. 4**) but limited differences in gel structure and storage modulus (**Fig. 2**, **Fig. S2**). The movement of embedded beads has previously been shown to correlate closely with traditional imaging of fiber displacement in collagen matrices, and thus bead mobility is a proxy for matrix deformations[38,39].

In all cases, spheroids exerted measurable traction forces on the gel within several hours, consistent with previous measurements of spheroids in or atop gels [39-41]. Following initial force generation, spheroids began to spread, with some cells migrating away from the spheroids. Qualitatively, cell shape was similar to that seen for dispersed cell spreading atop gels: both round and extended cells were seen, with a greater proportion of elongated cells seen on the high plasticity gels (Fig. 5). In all cases, the spheroids exerted forces on the gel directed inwards towards the spheroid, with beads in an area of approximately 1 mm² centered on the spheroid pulled over 20 hours an average of 7.2 \pm 4.4 μ m across spheroids (3 spheroids for each condition; $6.2 \pm 1.4 \, \mu m$ for the high concentration IPNs and $7.9 \pm 6.7 \, \mu m$ for the low concentration gels). This amount of matrix displacement at 20 hours is consistent with other studies of MDA-MB-231 spheroid spreading in 2D[39] as well as in 3D for other invasive cell types[40]. While cells exerted similar traction forces on both gel types, upon treatment with cytochalasin-D, a potent inhibitor of actin polymerization that causes cells to round up and release from the gels, differences in gel relaxation were apparent. In the high concentration (low plasticity) gels, beads moved back towards their original positions following cell treatment, with average relaxation distance of 3.8 ± 1.5 µm, corresponding to 38.7% plasticity on average. In contrast, the low concentration (high plasticity) gels showed very little relaxation, indicating significant irreversible deformation, with an average of 89.4% plasticity. Results from representative experiments showing bead motion during the pulling and relaxation phases on the two types of IPNs in a smaller (400 μm²) region adjacent to the spheroids are shown in Fig. 5.

These findings suggest that plasticity as measured via bulk creep and recovery tests reflect microscopic fiber behavior and is relevant for stresses cells may exert. Extrapolating from **Fig. 3**, these results suggest cells within and emerging from spheroids may produce stresses of > 20 Pa, consistent with some previous results of traction forces generated via collective migration [42] and spheroid wetting [43]. Additionally, these results support that cell-induced gel plasticity affects cell shape, presumably through a mechanism in which cell-mediated plastic deformation of the substrate provokes cellular polarization and elongation.

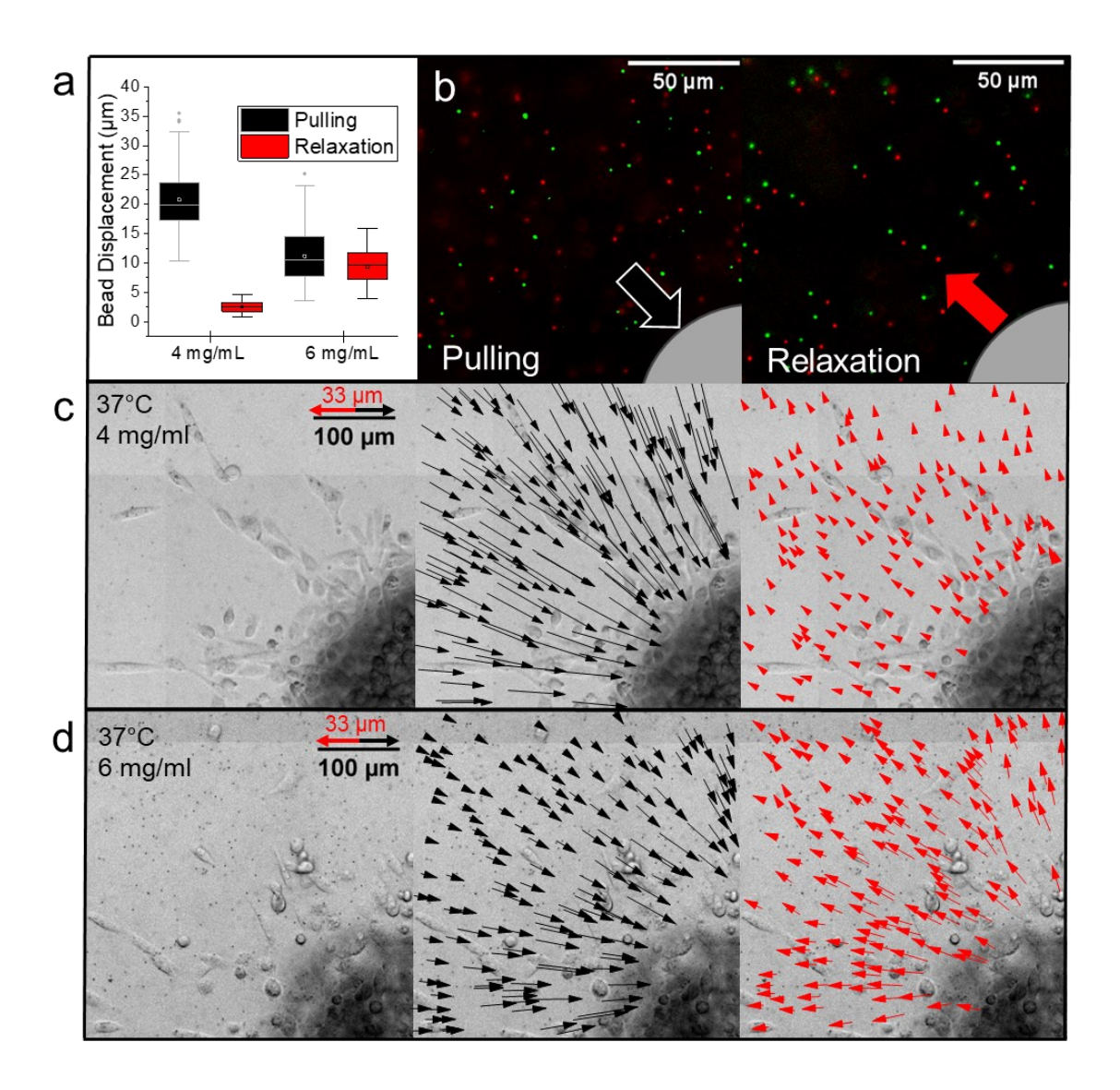


Figure 5. Spheroid Gel Deformation and Relaxation Experiments. a) Distribution of bead displacements in representative 37°C collagen-PEG IPNs during spheroid force generation (black) after 20 hours of incubation and relaxation (red) 2 hours after addition of relaxation solution. These distributions correspond to the bead displacements in areas shown in (c,d), with local plasticity of 88.0% and 15.3% in the low and high collagen concentration IPNs, respectively. b) Representative composite image of bead displacement during spheroid contraction in a high collagen concentration IPN. The bottom right arc represents the spheroid location with respect to the beads. Left: Red shows initial bead position and green shows bead position 20 hours after spheroid placement. Right: Red shows bead position after 20 hours of incubation and green shows bead position 2 hours after addition of the cell relaxation solution. c,d) Portion of representative spheroids spreading atop (c) a low collagen concentration 37°C IPN and (d) a high collagen concentration 37°C IPN. Left: Transmitted images of a portion of the spheroids. Middle: Vectors representing bead motion during spheroid contraction over 20 hours. Right: Vectors representing bead motion in the 2 hours following cell detachment. All vectors are displayed with the magnitude of displacement multiplied by a factor of 3, with vector tail placed at the original bead position such that the scale bar with arrows corresponds to bead motion while the other scale bar corresponds to real space.

4. DISCUSSION

This study demonstrates that collagen I gelation parameters can be utilized to modify structural, mechanical, and biofunctional properties of collagen-based IPNs. Here, we tuned collagen concentration and gelation temperature, which both affect collagen (and IPN) material properties. Consistent with previous studies, we show that collagen concentration and gelation temperature affect both network architecture and stiffness, with lower temperatures leading to thicker collagen fiber bundles, larger pore sizes, and stiffer gels. The effects of concentration and gelation temperature are maintained in the collagen-based IPNs despite the addition of the synthetic PEG network, allowing the tunable network architecture and biofunctionality of collagen gels to be preserved while increasing the storage modulus significantly, an important goal in some bioengineering applications and to better mimic mechanical properties of many tissues[5,15]. Collagen-IPN networks thus hold promise as highly tunable networks, as both the primary collagen and secondary synthetic network afford various opportunities for tunability.

The influence of collagen concentration and gelation temperature on plasticity is less obvious than their effects on microstructure and stiffness in both single component collagen gels and the IPNs. For collagen gels, it appears the plasticity of the gels depends primarily on the collagen concentration, while collagen concentration, gelation temperature, and the presence of PEG all affect plasticity of the IPNs. The IPNs have a broader range of plasticity than pure collagen gels, with the collagen gels tested showing plasticity ranging from 40-75% compared to the broader range found in the IPNs (20-90%). IPN systems designed with tunable plasticity often cover a much smaller range of plasticity than the IPNs described here and typically are more elastic than their biological component[44–46]. The enhanced range of plasticity of the IPNs studied here closely resembles that of actual soft tissues, which have been reported to range in plasticity from 20% for stiffer tissues like muscle to over 80% for the softest tissues such as kidney or brain[45].

Models of collagen plasticity[36,47] suggest that irreversible plastic deformation is caused by dynamic remodeling of collagen fibers as the weak physical crosslinks between fibers break and reform, and that permanent, covalent crosslinking of fibers substantially reduces plasticity[21]. Within this framework we would expect that the cross-linked PEG network entangled with the collagen network decreases plasticity in the IPNs relative to pure collagen networks by inhibiting fiber remodeling. Interestingly, while the two low concentration collagen gels exhibit similar plasticity as single-component networks, only the 37°C IPN become less plastic following reinforcement with PEG (**Fig. S4**). Given the aforementioned model of plastic deformation, this suggests that dynamic remodeling of the collagen network in the 37°C gels is more hindered by the addition of PEG than in the 15°C gels. It is possible that the higher fiber density in the 37°C gels creates tighter entanglements with the PEG network as compared to the 15°C gels, leading to the observed effect. This is further supported by the observation that the high concentration 15°C IPN is more plastic than the high concentration 37°C IPN.

The collagen-PEG IPNs investigated here were shown to modulate cell spreading based on the gelation conditions and resulting plasticity of the matrices. In recent years, matrix plasticity has entered into focus in the study of matrix-cell interactions alongside other factors such as pore size[26,28,29,48] and stiffness[49–52]. Several studies have found that matrix plasticity is important in cell spreading and migration on biomaterials including some that are collagen-based[21–24]. Wisdom et al. used a basement membrane (collagen IV)-alginate IPN with decoupled plasticity and stiffness, and Grolman et al. used an alginate-PEG system to decouple plasticity and stress relaxation, both showing that matrix plasticity facilitates cell spreading[22,23]. While the collagen-PEG system does not fully decouple plasticity from other mechanical

properties, our work suggests that matrix plasticity is a dominant factor in setting cell spreading on these gels relative to fiber density or storage modulus. This is supported by the fact that IPNs that show a greater degree of permanent deformation in creep and recovery tests also show this behavior in microscopic measurements with cell-induced stresses (**Fig. 5**). Additionally, recent work exploring the relationship between stiffness and cell spreading of MDA-MB-231 cells found no clear relationship between the two, even over a broad range of substrate stiffnesses[53]. The influence of collagen pore size and co-modulation with plasticity in determining cell behavior are yet to be explored, requiring additional experiments using 3D cell culture. The platform investigated here should prove suitable for such studies[9].

5. CONCLUSIONS

In this work, a collagen-based interpenetrating network hydrogel in which a PEG secondary network enhances the material's storage modulus and allows the material to sustain larger stresses is presented. These IPNs support cell spreading and span a wider range in plasticity than previously presented cell-compatible materials, thus more closely resembling tissue, while preserving the full structural tunability of collagen networks. Cell spreading was found to be modulated by IPN plasticity, with more plastic networks leading to enhanced cell spreading and elongation, consistent with previous findings. Microscopic measurements of matrix deformations due to cell generated forces reflected bulk measurements of plasticity. The IPNs developed and investigated here are suitable for applications requiring stronger cell culture materials, wider ranges of viscoelasticity, and mechanical control of cell spreading.

ACKNOWLEDGEMENTS

M.B.G. acknowledges the Walter A. '59 and Catherine R. Scott Research Fellowship and the National Science Foundation (DMR 2143146). We thank the Columbia University Department of Biology Imaging Facility for use of their microscopy equipment.

CONFLICT OF INTEREST

The authors declare no conflict of interest.

AUTHOR CONTRIBUTIONS

I.G.M., K.Y., A.J.D., M.B.G. and L.J.K. designed the research; I.G.M., M.B.G. and K.Y. performed experiments; I.G.M., K.Y., A.J.D. analyzed data; I.G.M., L.J.K. and M.B.G. wrote and edited the manuscript.

REFERENCES

- [1] L.H. Sperling, Interpenetrating Polymer Networks: An Overview, in: Interpenetr. Polym. Netw., American Chemical Society, 1994: pp. 3–38. https://doi.org/10.1021/ba-1994-0239.ch001.
- [2] E.S. Dragan, Design and applications of interpenetrating polymer network hydrogels. A review, Chem. Eng. J. 243 (2014) 572–590. https://doi.org/10.1016/j.cej.2014.01.065.
- [3] A.P. Dhand, J.H. Galarraga, J.A. Burdick, Enhancing Biopolymer Hydrogel Functionality through Interpenetrating Networks, Trends Biotechnol. 39 (2021) 519–538. https://doi.org/10.1016/j.tibtech.2020.08.007.
- [4] T.R. Anju, J. Sindhu Rachel, Biopolymer-Based Interpenetrating Polymer Networks, in: S. Thomas, AR, A., J. Chirayil, C., B. Thomas (Eds.), Handb. Biopolym., Springer, Singapore, 2023
- [5] E. Rezvani Ghomi, N. Nourbakhsh, M. Akbari Kenari, M. Zare, S. Ramakrishna, Collagen-based biomaterials for biomedical applications, J. Biomed. Mater. Res. B Appl. Biomater. 109 (2021) 1986–1999. https://doi.org/10.1002/jbm.b.34881.
- [6] J. Lou, R. Stowers, S. Nam, Y. Xia, O. Chaudhuri, Stress relaxing hyaluronic acid-collagen hydrogels promote cell spreading, fiber remodeling, and focal adhesion formation in 3D cell culture, Biomaterials 154 (2018) 213–222. https://doi.org/10.1016/j.biomaterials.2017.11.004.
- [7] C. Branco da Cunha, D.D. Klumpers, W.A. Li, S.T. Koshy, J.C. Weaver, O. Chaudhuri, P.L. Granja, D.J. Mooney, Influence of the stiffness of three-dimensional alginate/collagen-l interpenetrating networks on fibroblast biology, Biomaterials 35 (2014) 8927–8936. https://doi.org/10.1016/j.biomaterials.2014.06.047.
- [8] D.J. Munoz-Pinto, A.C. Jimenez-Vergara, T.P. Gharat, M.S. Hahn, Characterization of sequential collagen-poly(ethylene glycol) diacrylate interpenetrating networks and initial assessment of their potential for vascular tissue engineering, Biomaterials 40 (2015) 32–42. https://doi.org/10.1016/j.biomaterials.2014.10.051.
- [9] D.S. Reynolds, K.M. Bougher, J.H. Letendre, S.F. Fitzgerald, U.O. Gisladottir, M.W. Grinstaff, M.H. Zaman, Mechanical confinement via a PEG/Collagen interpenetrating network inhibits behavior characteristic of malignant cells in the triple negative breast cancer cell line MDA.MB.231, Acta Biomater. 77 (2018) 85–95. https://doi.org/10.1016/j.actbio.2018.07.032.
- [10] T.D. Sargeant, A.P. Desai, S. Banerjee, A. Agawu, J.B. Stopek, An in situ forming collagen–PEG hydrogel for tissue regeneration, Acta Biomater. 8 (2012) 124–132. https://doi.org/10.1016/j.actbio.2011.07.028.
- [11] J. Elango, C. Hou, B. Bao, S. Wang, J.E. Maté Sánchez de Val, W. Wenhui, The Molecular Interaction of Collagen with Cell Receptors for Biological Function, Polymers 14 (2022) 876. https://doi.org/10.3390/polym14050876.
- [12] J. Xie, M. Bao, S.M.C. Bruekers, W.T.S. Huck, Collagen Gels with Different Fibrillar Microarchitectures Elicit Different Cellular Responses, ACS Appl. Mater. Interfaces 9 (2017) 19630–19637. https://doi.org/10.1021/acsami.7b03883.
- [13] M.D. Shoulders, R.T. Raines, COLLAGEN STRUCTURE AND STABILITY, Annu. Rev. Biochem. 78 (2009) 929–958. https://doi.org/10.1146/annurev.biochem.77.032207.120833.
- [14] K.E. Kadler, Y. Hojima, D.J. Prockop, Assembly of collagen fibrils de novo by cleavage of the type I pC-collagen with procollagen C-proteinase. Assay of critical concentration demonstrates that collagen self-assembly is a classical example of an entropy-driven process., J. Biol. Chem. 262 (1987) 15696–15701. https://doi.org/10.1016/S0021-9258(18)47783-6.
- [15] E.E. Antoine, P.P. Vlachos, M.N. Rylander, Review of Collagen I Hydrogels for Bioengineered Tissue Microenvironments: Characterization of Mechanics, Structure, and

- Transport, Tissue Eng. Part B Rev. 20 (2014) 683–696. https://doi.org/10.1089/ten.teb.2014.0086.
- [16] C.B. Raub, J. Unruh, V. Suresh, T. Krasieva, T. Lindmo, E. Gratton, B.J. Tromberg, S.C. George, Image Correlation Spectroscopy of Multiphoton Images Correlates with Collagen Mechanical Properties, Biophys. J. 94 (2008) 2361–2373. https://doi.org/10.1529/biophysj.107.120006.
- [17] C.B. Raub, V. Suresh, T. Krasieva, J. Lyubovitsky, J.D. Mih, A.J. Putnam, B.J. Tromberg, S.C. George, Noninvasive Assessment of Collagen Gel Microstructure and Mechanics Using Multiphoton Microscopy, Biophys. J. 92 (2007) 2212–2222. https://doi.org/10.1529/biophysj.106.097998.
- [18] M. Achilli, D. Mantovani, Tailoring Mechanical Properties of Collagen-Based Scaffolds for Vascular Tissue Engineering: The Effects of pH, Temperature and Ionic Strength on Gelation, Polymers 2 (2010) 664–680. https://doi.org/10.3390/polym2040664.
- [19] Y. Yang, L.M. Leone, L.J. Kaufman, Elastic Moduli of Collagen Gels Can Be Predicted from Two-Dimensional Confocal Microscopy, Biophys. J. 97 (2009) 2051–2060. https://doi.org/10.1016/j.bpj.2009.07.035.
- [20] Y. Yang, S. Motte, L.J. Kaufman, Pore size variable type I collagen gels and their interaction with glioma cells, Biomaterials 31 (2010) 5678–5688. https://doi.org/10.1016/j.biomaterials.2010.03.039.
- [21] S. Nam, J. Lee, D. Brownfield, O. Chaudhuri, Viscoplasticity Enables Mechanical Remodeling of Matrix by Cells, Biophys. J. 111 (2016) 2296-2308. https://doi.org/10.1016/j.bpj.2016.10.002.
- [22] K.M. Wisdom, K. Adebowale, J. Chang, J.Y. Lee, S. Nam, R. Desai, N.S. Rossen, M. Rafat, R.B. West, L. Hodgson, O. Chaudhuri, Matrix mechanical plasticity regulates cancer cell migration through confining microenvironments, Nat. Commun. 9 (2018) 4144. https://doi.org/10.1038/s41467-018-06641-z.
- [23] J.M. Grolman, P. Weinand, D.J. Mooney, Extracellular matrix plasticity as a driver of cell spreading, Proc. Natl. Acad. Sci. 117 (2020) 25999–26007. https://doi.org/10.1073/pnas.2008801117.
- [24] O. Chaudhuri, J. Cooper-White, P.A. Janmey, D.J. Mooney, V.B. Shenoy, Effects of extracellular matrix viscoelasticity on cellular behaviour, Nature 584 (2020) 535–546. https://doi.org/10.1038/s41586-020-2612-2.
- [25] K.M. Warren, Md.M. Islam, P.R. LeDuc, R.Jr. Steward, 2D and 3D Mechanobiology in Human and Nonhuman Systems, ACS Appl. Mater. Interfaces 8 (2016) 21869–21882. https://doi.org/10.1021/acsami.5b12064.
- [26] I. Bružauskaitė, D. Bironaitė, E. Bagdonas, E. Bernotienė, Scaffolds and cells for tissue regeneration: different scaffold pore sizes—different cell effects, Cytotechnology 68 (2016) 355–369. https://doi.org/10.1007/s10616-015-9895-4.
- [27] F. Geiger, D. Rüdiger, S. Zahler, H. Engelke, Fiber stiffness, pore size and adhesion control migratory phenotype of MDA-MB-231 cells in collagen gels, PLOS ONE 14 (2019) e0225215. https://doi.org/10.1371/journal.pone.0225215.
- [28] S.-M. Lien, L.-Y. Ko, T.-J. Huang, Effect of pore size on ECM secretion and cell growth in gelatin scaffold for articular cartilage tissue engineering, Acta Biomater. 5 (2009) 670–679. https://doi.org/10.1016/j.actbio.2008.09.020.
- [29] A. Guzman, M.J. Ziperstein, L.J. Kaufman, The effect of fibrillar matrix architecture on tumor cell invasion of physically challenging environments, Biomaterials 35 (2014) 6954– 6963. https://doi.org/10.1016/j.biomaterials.2014.04.086.
- [30] J. Kalia, R.T. Raines, Advances in Bioconjugation, Curr. Org. Chem. 14 (2010) 138–147. https://doi.org/10.2174/138527210790069839.
- [31] N. Stephanopoulos, M.B. Francis, Choosing an effective protein bioconjugation strategy, Nat. Chem. Biol. 7 (2011) 876–884. https://doi.org/10.1038/nchembio.720.

- [32] L.J. Kaufman, C.P. Brangwynne, K.E. Kasza, E. Filippidi, V.D. Gordon, T.S. Deisboeck, D.A. Weitz, Glioma Expansion in Collagen I Matrices: Analyzing Collagen Concentration-Dependent Growth and Motility Patterns, Biophys. J. 89 (2005) 635–650. https://doi.org/10.1529/biophysi.105.061994.
- [33] A. Narayanan, A. Rajan, R. Pramanik, A. Arockiarajan, A thermodynamically-consistent phenomenological viscoplastic model for hydrogels, Mater. Res. Express 6 (2019) 085418. https://doi.org/10.1088/2053-1591/ab2a49.
- [34] S. Bhattacharya, R. Shunmugam, Unraveling the Effect of PEG Chain Length on the Physical Properties and Toxicant Removal Capacities of Cross-Linked Network Synthesized by Thiol–Norbornene Photoclick Chemistry, ACS Omega 5 (2020) 2800– 2810. https://doi.org/10.1021/acsomega.9b03554.
- [35] K. Menard, Dynamic Mechanical Analysis: A Practical Introduction, CRC Press, 1999. https://doi.org/10.1201/9781420049183.
- [36] E. Ban, J.M. Franklin, S. Nam, L.R. Smith, H. Wang, R.G. Wells, O. Chaudhuri, J.T. Liphardt, V.B. Shenoy, Mechanisms of Plastic Deformation in Collagen Networks Induced by Cellular Forces, Biophys. J. 114 (2018) 450–461. https://doi.org/10.1016/j.bpj.2017.11.3739.
- [37] R.E. Bird, S.A. Lemmel, X. Yu, Q.A. Zhou, Bioorthogonal Chemistry and Its Applications, Bioconjug. Chem. 32 (2021) 2457–2479. https://doi.org/10.1021/acs.bioconjchem.1c00461.
- [38] E. Tamariz, F. Grinnell, Modulation of Fibroblast Morphology and Adhesion during Collagen Matrix Remodeling, Mol. Biol. Cell 13 (2002) 3915–3929. https://doi.org/10.1091/mbc.E02-05-0291.
- [39] E. Blauth, S. Grosser, F. Sauer, M. Merkel, H. Kubitschke, E. Warmt, E.W. Morawetz, P. Friedrich, B. Wolf, S. Briest, G.G.R. Hiller, L.-C. Horn, B. Aktas, J.A. Käs, Different contractility modes control cell escape from multicellular spheroids and tumor explants, APL Bioeng. 8 (2024) 026110. https://doi.org/10.1063/5.0188186.
- [40] K.S. Kopanska, Y. Alcheikh, R. Staneva, D. Vignjevic, T. Betz, Tensile Forces Originating from Cancer Spheroids Facilitate Tumor Invasion, PLoS One 11 (2016) e0156442. https://doi.org/10.1371/journal.pone.0156442.
- [41] C. Mark, T.J. Grundy, P.L. Strissel, D. Böhringer, N. Grummel, R. Gerum, J. Steinwachs, C.C. Hack, M.W. Beckmann, M. Eckstein, R. Strick, G.M. O'Neill, B. Fabry, Collective forces of tumor spheroids in three-dimensional biopolymer networks, eLife 9 (2020) e51912. https://doi.org/10.7554/eLife.51912.
- [42] X. Trepat, M.R. Wasserman, T.E. Angelini, E. Millet, D.A. Weitz, J.P. Butler, J.J. Fredberg, Physical forces during collective cell migration, Nat. Phys. 5 (2009) 426–430. https://doi.org/10.1038/nphys1269.
- [43] C. Pérez-González, R. Alert, C. Blanch-Mercader, M. Gómez-González, T. Kolodziej, E. Bazellieres, J. Casademunt, X. Trepat, Active wetting of epithelial tissues, Nat. Phys. 15 (2019) 79–88. https://doi.org/10.1038/s41567-018-0279-5.
- [44] K.M. Wisdom, D. Indana, P.-E. Chou, R. Desai, T. Kim, O. Chaudhuri, Covalent cross-linking of basement membrane-like matrices physically restricts invasive protrusions in breast cancer cells, Matrix Biol. 85–86 (2020) 94–111. https://doi.org/10.1016/j.matbio.2019.05.006.
- [45] Z. Wei, M. Lei, Y. Wang, Y. Xie, X. Xie, D. Lan, Y. Jia, J. Liu, Y. Ma, B. Cheng, S. Gerecht, F. Xu, Hydrogels with tunable mechanical plasticity regulate endothelial cell outgrowth in vasculogenesis and angiogenesis, Nat. Commun. 14 (2023) 8307. https://doi.org/10.1038/s41467-023-43768-0.
- [46] Y. Jia, Y. Wang, L. Niu, H. Zhang, J. Tian, D. Gao, X. Zhang, T.J. Lu, J. Qian, G. Huang, F. Xu, The Plasticity of Nanofibrous Matrix Regulates Fibroblast Activation in Fibrosis, Adv. Healthc. Mater. 10 (2021) 2001856. https://doi.org/10.1002/adhm.202001856.

- [47] J. Kim, J. Feng, C.A.R. Jones, X. Mao, L.M. Sander, H. Levine, B. Sun, Stress-induced plasticity of dynamic collagen networks, Nat. Commun. 8 (2017) 842. https://doi.org/10.1038/s41467-017-01011-7.
- [48] A. Matsiko, J.P. Gleeson, F.J. O'Brien, Scaffold Mean Pore Size Influences Mesenchymal Stem Cell Chondrogenic Differentiation and Matrix Deposition, Tissue Eng. Part A 21 (2015) 486–497. https://doi.org/10.1089/ten.tea.2013.0545.
- [49] R.J. Pelham, Y. Wang, Cell locomotion and focal adhesions are regulated by substrate flexibility, Proc. Natl. Acad. Sci. 94 (1997) 13661–13665. https://doi.org/10.1073/pnas.94.25.13661.
- [50] A.J. Engler, S. Sen, H.L. Sweeney, D.E. Discher, Matrix Elasticity Directs Stem Cell Lineage Specification, Cell 126 (2006) 677–689. https://doi.org/10.1016/j.cell.2006.06.044.
- [51] M.H. Zaman, L.M. Trapani, A.L. Sieminski, D. MacKellar, H. Gong, R.D. Kamm, A. Wells, D.A. Lauffenburger, P. Matsudaira, Migration of tumor cells in 3D matrices is governed by matrix stiffness along with cell-matrix adhesion and proteolysis, Proc. Natl. Acad. Sci. 103 (2006) 10889–10894. https://doi.org/10.1073/pnas.0604460103.
- [52] R.G. Wells, The role of matrix stiffness in regulating cell behavior, Hepatology 47 (2008) 1394–1400. https://doi.org/10.1002/hep.22193.
- [53] V.S. Rozova, A.G. Anwer, A.E. Guller, H.A. Es, Z. Khabir, A.I. Sokolova, M.U. Gavrilov, E.M. Goldys, M.E. Warkiani, J.P. Thiery, A.V. Zvyagin, Machine learning reveals mesenchymal breast carcinoma cell adaptation in response to matrix stiffness, PLoS Comput. Biol. 17 (2021) e1009193. https://doi.org/10.1371/journal.pcbi.1009193.